

Absolutely continuous energy bands and extended electronic states in an aperiodic comb-shaped nanostructure

Biplab Pal*

Department of Physics, University of Kalyani, Kalyani, West Bengal-741235, India

The nature of electronic eigenstates and quantum transport in a comb-shaped Fibonacci nanostructure model is investigated within a tight-binding framework. Periodic linear chains are side-attached to a Fibonacci chain, giving it the shape of an aperiodic comb. The effect of the side-attachments on the usual Cantor set energy spectrum of a Fibonacci chain is analyzed using the Greens function technique. A special correlation between the coupling of the side-attached chain with the Fibonacci chain and the inter-atomic coupling of the Fibonacci chain results in a dramatic triggering of the fragmented Cantor set energy spectrum into multiple sets of continuous sub-bands of extended eigenstates. The result is valid even for a disordered comb and turns out to be a rare exception of the conventional Anderson localization problem. The electronic transport thus can be made selectively ballistic within desired energy regimes. The number and the width of such continuous sub-bands can be easily controlled by tuning the number of atomic sites in the side-coupled periodic linear chains. This gives us a scope of proposing such aperiodic nanostructures as potential candidates for prospective energy selective nanoscale filtering devices.

PACS numbers: 61.44.-n, 73.20.Jc, 73.22.Dj, 73.63.-b

Keywords: Aperiodic nanostructure, Single electron states, Quantum transport, Tight-binding model

I. INTRODUCTION

Fano-Anderson effect is an interesting phenomenon exhibited by excitonic states in a tight binding lattice when a discrete, bound state ‘interacts’ with a continuum [1–12]. The effect is explicitly seen when one considers transmission spectrum of one dimensional quantum wire (QW) systems with a single quantum dot (QD), or a cluster of them is attached to the QW from one side [7, 8, 10, 11]. Needless to say, the studies so far has gone well beyond mere theoretical interest, thanks to the present advanced stage of lithographic techniques and nanotechnology, and has incorporated the studies of nonequilibrium dynamics in optical transition [13], quantum simulation [14] and tunneling in a Kondo hole system [15] to name a few.

In spite of the considerable volume of work existing in this field, a practically unaddressed issue, to the best of our knowledge, is how seriously does the presence of *bound states* caused by the attachment (from one side) of a QD or an assembly of them, influence a singular continuous spectrum. A singular continuous spectrum is the hallmark of what are known as quasiperiodic systems [16–20] such as the Fibonacci class of substitutionally generated atomic chains or, the array of Harper potentials (Aubry-Andre chains). Due to the fragmented, Cantor like character of the energy spectra offered by these systems, the bound states can, in principle, occupy any local gap inside the spectrum and may de-stabilize the fundamental character of the entire energy spectrum. A central motivation of the present work is to look into such an issue.

We intend to work with a golden mean Fibonacci chain where finite arrays of QDs are side-grafted to every atomic site, giving the lattice an aperiodic comb structure. The model has particular relevance in the context of recent studies on spectral properties of excitons in nanoparticle array [21–25]. The comb-structure enables us to examine the interference of Fano lineshapes and the effect of the side coupled dots on the energy spectrum and transport properties of such a system. The presence of multiple, closely spaced gaps and a multifractal spectrum, when coupled to discrete, bound states from one side, offers a possibility of controlling the gaps, and may be even the basic character of the electronic states. In the present day of nanotechnology and revolution in fabricating tailor made lattices this can even open up the possibility of designing novel QD devices. These aspects prompt us to undertake the present study.

We find extremely interesting results. With a golden mean Fibonacci chain having side coupled QD arrays, the presence of an infinite number of grafted chains enables one to control the transmission properties at all scales of energy by suitably changing the number of atoms in the side coupled array. The most important result is that, under certain special conditions the entire energy spectrum of the infinite system turns out to have absolutely continuous subbands of energy. The occurrence of these continuous subbands is triggered by a certain special relationship between the off-diagonal elements of the Hamiltonian. Surprisingly, this is something that is not expected in any conventional localization scheme, such as the Anderson localization [26], where the single particle states get localized in a disordered array of potentials irrespective of the numerical values of the parameters of the Hamiltonian. Our results therefore present a strong case of a violation of this *universality* of Anderson localization.

*Electronic address: biplabpal@klyuniv.ac.in

The system to be described by a tight-binding Hamiltonian, is depicted in Fig. 1. We have used real space renormalization group (RSRG) decimation scheme [27] and Green's function technique to analyze the energy spectrum and the nature of eigenstates of the system. The side-attached QD arrays play a crucial role in generating and controlling the number of continuous energy bands. Extended character of the electron states populated in the bands are reflected in a prominent enhancement of two-terminal quantum transport through the system.

In what follows, we describe the results obtained by us. In section II we present our model and the mathematical methods used for handling the problem. The effect of the side-attachment on the energy spectrum of the system and how to obtain the condition for generating absolutely continuous bands of extended states is discussed in section III. Section IV presents the two-terminal transmission characteristics of the system, and finally in section V we draw our conclusion with possible applications for future study.

II. DESCRIPTION OF THE MODEL AND THE METHOD

A. The system and the Hamiltonian

Fig. 1 illustrates our system of interest. We have considered a model quasiperiodic nanostructure, in which atomic sites are arranged following a Fibonacci sequence on a linear chain (the backbone) and periodic, finite sized QD arrays are side-attached to the backbone forming an aperiodic comb-shaped system. The Fibonacci chain is

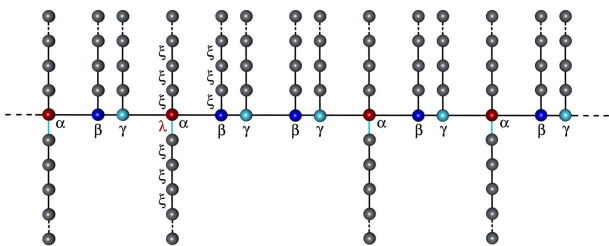


FIG. 1: (Color online) Schematic diagram of a model quasiperiodic nanostructure. Sites in the backbone are named and colored differently to distinguish between nearest neighbor bond environments. α , β , and γ sites are side-attached with finite size periodic QD arrays, while each α site has an extra dangling QD chain coupled to it through a coupling strength λ .

grown recursively by repeated application of the inflation rule [16, 18] $L \rightarrow LS$ and $S \rightarrow L$, where L and S stand for two ‘‘bonds’’, viz., long bond and short bond respectively. The first few generations are,

$$G_1:L, G_2:LS, G_3:LSL, G_4:LSLLS$$

and so on. The number of L bonds and the number of S bonds bear the golden ratio $\tau = (\sqrt{5} + 1)/2$ in the thermodynamic limit.

Depending on the nearest neighbor bond environment, we identify three kinds of sites, viz., α (red dots), β (dark blue dots), and γ (light blue dots) – flanked by L - L , L - S and S - L bonds respectively as shown in Fig. 1. Periodic finite QD arrays of identical size (having $N + 1$ QDs in each array) are side-attached to every α , β , and γ sites, while an extra QD array of size $N + 2$ is hung from each α site, which couples to it through a coupling strength λ as shown in Fig. 1, N being any positive integer. We adopt a tight-binding formalism and incorporate only nearest neighbor hopping. Within the framework of non-interacting electron picture, the tight-binding Hamiltonian of the system can be expressed as,

$$\mathbf{H} = \mathbf{H}_{backbone} + \mathbf{H}_{upperchains} + \mathbf{H}_{lowerchains} + \mathbf{H}_{backbone-upperchains} + \mathbf{H}_{backbone-lowerchains} \quad (1)$$

where,

$$\mathbf{H}_{backbone} = \sum_i \epsilon_i c_i^\dagger c_i + \sum_{\langle ij \rangle} (t_{ij} c_i^\dagger c_j + h.c.)$$

$$\mathbf{H}_{upperchains} = \sum_{\alpha, \beta, \gamma \text{ sites}} \left[\sum_{\mu=1}^{N+1} \epsilon_\mu d_\mu^\dagger d_\mu + \sum_{\langle \mu\nu \rangle} (t_{\mu\nu} d_\mu^\dagger d_\nu + h.c.) \right]$$

$$\mathbf{H}_{lowerchains} = \sum_{\alpha \text{ sites}} \left[\sum_{\mu=1}^{N+2} \epsilon_\mu d_\mu^\dagger d_\mu + \sum_{\langle \mu\nu \rangle} (t_{\mu\nu} d_\mu^\dagger d_\nu + h.c.) \right]$$

$$\mathbf{H}_{backbone-upperchains} = \sum_{\alpha, \beta, \gamma \text{ sites}} \xi (c_i^\dagger d_1 + d_1^\dagger c_i)$$

$$\mathbf{H}_{backbone-lowerchains} = \sum_{\alpha \text{ sites}} \lambda (c_i^\dagger d_1 + d_1^\dagger c_i)$$

In the above, $c_i^\dagger (c_i)$ and $d_\mu^\dagger (d_\mu)$ represent the creation (annihilation) operators for the backbone and dangling QD arrays respectively. ϵ_i is the on-site potential of an i -th atomic site along the Fibonacci backbone of the lattice, which may take three different values, viz., ϵ_α , ϵ_β , and ϵ_γ corresponding to three different kinds of sites as mentioned above. The nearest neighbor hopping integral t_{ij} takes two values t_L and t_S for electron hopping along the L and S bond respectively. ϵ_μ is the value of on-site energy at an atomic site in the dangling chains, which will assume a constant value equal to ϵ_0 for all the QDs in an array. The hopping integral along a dangling QD array also assumes a constant value $t_{\mu\nu} = \xi$, and λ is the coupling strength of the extra QD arrays coupled to each α -site.

B. Renormalization into an effective system

The dangling chains are ‘‘folded back’’ into the backbone using a RSRG decimation scheme [28]. As a result, the on-site energy of the renormalized atomic sites gets

dressed up, which we may call a kind of “self energy” of the effective atomic sites. This is demonstrated pictori-

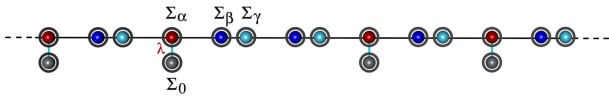


FIG. 2: (Color online) Schematic view of renormalized version of the original system. The side-attached dangling QD arrays are folded into effective atomic sites shown by encircled dots.

ally in Fig. 2 and the renormalized on-site potentials of the effective sites are given by,

$$\begin{aligned}\Sigma_\alpha &= \epsilon_\alpha + \Delta \\ \Sigma_\beta &= \epsilon_\beta + \Delta \\ \Sigma_\gamma &= \epsilon_\gamma + \Delta \\ \Sigma_0 &= \epsilon_0 + \Delta\end{aligned}\quad (2)$$

In the above equations, Δ is the term which contains the entire information about the folded periodic finite size QD arrays and is given by,

$$\Delta = \frac{\xi(E - \epsilon_0)U_{N-1}(x) - \xi^2 U_{N-2}(x)}{(E - \epsilon_0)U_N(x) - \xi U_{N-1}(x)}, \quad \text{for } N \geq 1 \quad (3)$$

where, $U_N(x) = 2xU_{N-1}(x) - U_{N-2}(x)$, for $N \geq 1$ is the Chebyshev polynomial of second kind, with $U_{-1} = 0$, $U_0 = 1$, and $x = 1/2[\text{Tr}(\mathbf{M})]$, \mathbf{M} being the 2×2 transfer matrix of the form,

$$\mathbf{M} = \begin{pmatrix} (E - \epsilon_0)/\xi & -1 \\ 1 & 0 \end{pmatrix}$$

for the atomic sites in the QD arrays.

Now we have a renormalized system with effective atomic sites arranged in a Fibonacci order along the backbone and each effective α -sites is now coupled to an effective dangling QD through a coupling strength λ (Fig. 2). We can easily decimate out the dangling “effective” QD, which will make the system into an effective 1-d Fibonacci array of renormalized atomic sites with renormalized on-site potentials, viz., $\tilde{\epsilon}_\alpha = \Sigma_\alpha + \lambda^2/(E - \Sigma_0)$, $\tilde{\epsilon}_\beta = \Sigma_\beta$, and $\tilde{\epsilon}_\gamma = \Sigma_\gamma$ as depicted in Fig. 3. Actually the

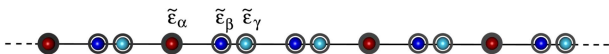


FIG. 3: (Color online) Effective 1-d Fibonacci array of atomic sites obtained by decimating the dangling renormalized QDs at the α -sites in figure 2.

on-site potentials at the β and γ sites do not get modified, but the to make the notations consistent we have renamed Σ_β and Σ_γ as $\tilde{\epsilon}_\beta$ and $\tilde{\epsilon}_\gamma$ respectively.

Using the Fibonacci growth-rule in the reverse direction it is simple to rescale any generation of the effective 1-d Fibonacci system into its earlier generation [27]. The

renormalized values of the on-site energy and hopping integrals can be expressed by the following relations:

$$\begin{aligned}\tilde{\epsilon}_\alpha(n+1) &= \tilde{\epsilon}_\alpha(n) + \frac{t_L^2(n) + t_S^2(n)}{E - \tilde{\epsilon}_\beta(n)} \\ \tilde{\epsilon}_\beta(n+1) &= \tilde{\epsilon}_\beta(n) + \frac{t_S^2(n)}{E - \tilde{\epsilon}_\beta(n)} \\ \tilde{\epsilon}_\gamma(n+1) &= \tilde{\epsilon}_\gamma(n) + \frac{t_L^2(n)}{E - \tilde{\epsilon}_\beta(n)} \\ t_L(n+1) &= \frac{t_L(n)t_S(n)}{E - \tilde{\epsilon}_\beta(n)} \\ t_S(n+1) &= t_L(n)\end{aligned}\quad (4)$$

where, n indicates the stage of renormalization. These recursion relations are used to obtain the energy spectrums of the system and are presented in the next the section.

III. ENERGY SPECTRUMS OF THE SYSTEM

A. Condition for obtaining the absolutely continuous bands

The renormalized effective 1-d Fibonacci chain is described by a set of three transfer matrices [18], viz., \mathbf{M}_α , \mathbf{M}_β , and \mathbf{M}_γ . The expressions for the three transfer matrices are,

$$\begin{aligned}\mathbf{M}_\alpha &= \begin{pmatrix} (E - \tilde{\epsilon}_\alpha)/t_L & -1 \\ 1 & 0 \end{pmatrix} \\ \mathbf{M}_\beta &= \begin{pmatrix} (E - \tilde{\epsilon}_\beta)/t_S & -t_L/t_S \\ 1 & 0 \end{pmatrix} \\ \mathbf{M}_\gamma &= \begin{pmatrix} (E - \tilde{\epsilon}_\gamma)/t_L & -t_S/t_L \\ 1 & 0 \end{pmatrix}\end{aligned}\quad (5)$$

and, \mathbf{M}_α and $\mathbf{M}_{\gamma\beta} = \mathbf{M}_\gamma \mathbf{M}_\beta$ follow an arrangement in the Fibonacci sequence. It can be easily verified that, if we choose $\epsilon_\alpha = \epsilon_\beta = \epsilon_\gamma = \epsilon_0$ and $t_L \neq t_S$, then the commutator $[\mathbf{M}_\alpha, \mathbf{M}_{\gamma\beta}]$ vanishes *irrespective of the energy* E , if we set $\lambda = \sqrt{t_S^2 - t_L^2}$. So, under this condition, when the transfer matrices corresponding to α clusters and the β - γ clusters commute, they can be arranged in any desired fashion, say, for example, in a perfectly periodic pattern. The spectrum offered by a periodic arrangement of building blocks is an absolutely continuous one. Once the commutator $[\mathbf{M}_\alpha, \mathbf{M}_{\gamma\beta}]$ is made to vanish, the entire Fibonacci lattice can be thought to be equivalent with two periodic infinite sub-lattices, one comprising the “renormalized” α -sites alone, and the other formed by a periodically repeating cluster of $\beta\gamma$ pairs. Each subsystem has its own continuous energy spectrum with a band-multiplicity that arises out of the

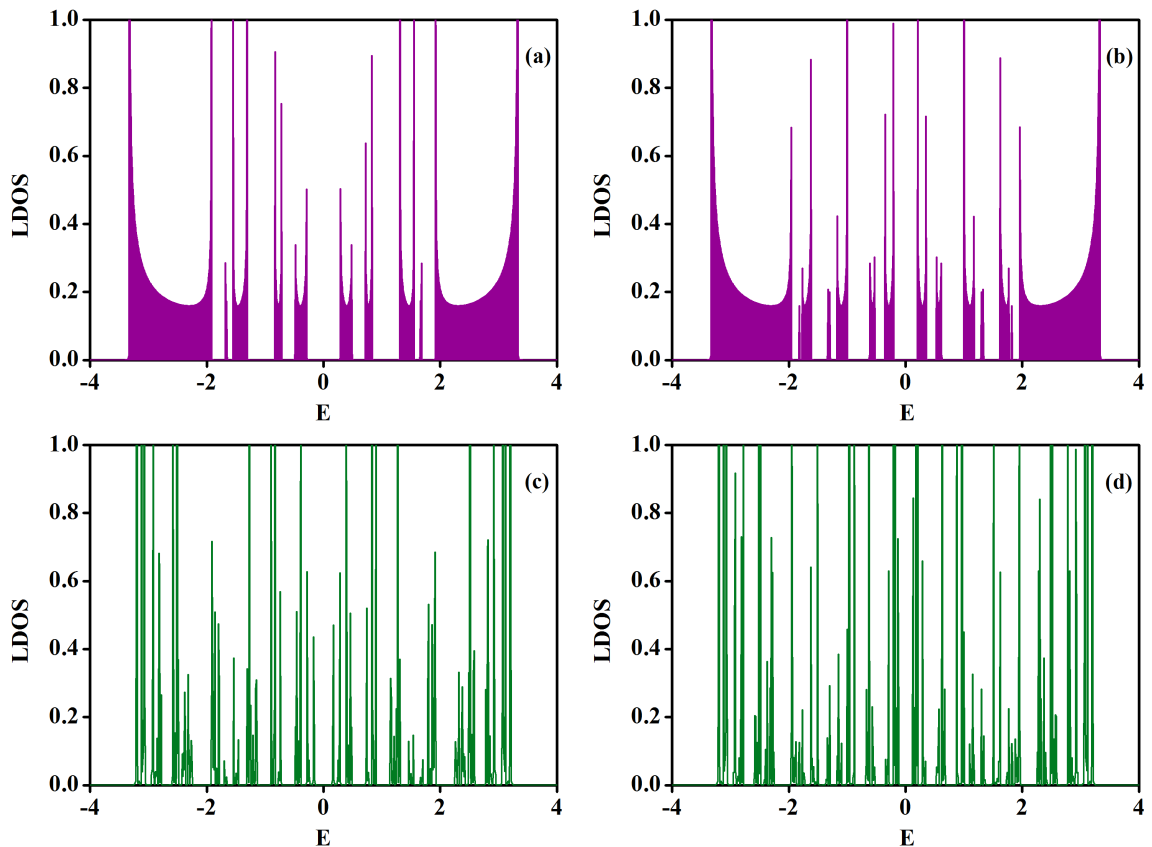


FIG. 4: (Color online) LDOS- E spectrum at an α -site of the system. The upper panel shows the LDOS- E spectrum under the suitable resonance condition, while the lower panel represents the LDOS- E spectrum for a 50% deviation from the desired resonance condition. In (a) and (c) number of atomic sites in each lower chain is 5 and in each upper chain is 4, while for (b) and (d) those are set equal to 7 and 6 respectively. The values of other parameters are $\epsilon_\alpha = \epsilon_\beta = \epsilon_\gamma = \epsilon_0 = 0$, $t_L = 1$, $t_S = 2$, and $\xi = 1$. For upper panel value of $\lambda = \sqrt{3}$, and for lower panel $\lambda = \sqrt{3}/2$ which is a 50% deviation from the resonance value.

side-coupled QD array. Most interestingly, the separate band structure arising in these two cases map onto each other, giving rise to a unique, absolutely continuous energy spectrum as verified by an extensive numerical work. This conclusively leads to the existence of a dense, gapless set of extended eigenfunctions when the resonance condition is satisfied. The fragmented, multifractal character of a typical Fibonacci quasicrystal disappears and all the eigenstates populating the continuous subbands are of extended character.

B. Local density of states

The local density of states (LDOS) at an α , β or γ is obtained by calculating the respective local Green's function $G_{00}^i = (E + i\delta - \epsilon_i^*)^{-1}$, where, $i = \alpha, \beta$ or γ . δ is a very small imaginary part added to the energy E , and ϵ_i^* represents the fixed point value of the respective on-site potential as the hopping integrals flows to zero under RSRG iterations of Eq. (4). The LDOS is given

by,

$$\rho_i(E) = \lim_{\delta \rightarrow 0} \left[-\frac{1}{\pi} \text{Im} (G_{00}^i) \right] \quad (6)$$

The results are presented in Fig. 4. We have verified that the LDOS at an α , or β , or γ site turns out to be the same. So to save space we have presented the LDOS at an α -site only. In the upper panel of Fig. 4, we have shown the LDOS at an α -site under the resonance condition. We have set $\epsilon_\alpha = \epsilon_\beta = \epsilon_\gamma = \epsilon_0 = 0$, $t_L = 1$, $t_S = 2$, $\xi = 1$, and $\lambda = \sqrt{3}$. As we set $\lambda = \sqrt{3}$, which satisfies the desired condition for matrix commutation as described in Sec. III A, it triggers absolutely continuous subbands in the energy spectra (Fig. 4(a) and (b)).

We have minutely examined each of these continuum sub-bands for a very fine scanning of the energy interval, and the continua still persist. This confirms the robustness of these continuum subbands under the resonance condition. The values of the hopping integrals t_L and t_S remains non-zero over arbitrarily large number of RSRG iteration steps for any energy inside each of these continuous subbands. This proves the extended nature of the electronic eigenstates in each of these subbands.

This fact is corroborated by a prominent enhancement of two-terminal transport through the system under the resonance condition which will be described in section IV. The number and the position of such subbands are sensitive to number of atomic sites in the side-attached chains. This fact is elucidated in Fig. 4(a) and (b). In Fig. 4(a), number of sites in each lower chain is set equal to 5 and in each upper chain is set equal to 4 respectively, and for Fig. 4(b) these are 7 and 6 respectively. Clearly, the number and position of subbands in the two cases change.

As we turn away from the resonance condition, the continua in the energy spectra get destroyed, and the typical Cantor set singular continuous energy spectra of a quasiperiodic system returns. This is shown in the lower panel panel of Fig. 4, where we have set $\lambda = \sqrt{3}/2$ which is a 50% deviation from its resonance value. All other parameters remain same as in upper panel of Fig. 4. However, isolated extended states still exists in such cases. These can be evaluated exactly.

C. The energy eigenvalue distribution

We have explored the energy eigenvalue distribution (Fig. 5) as a function of the coupling strength λ of the dangling chains with the α -sites. Fig. 5 is representative

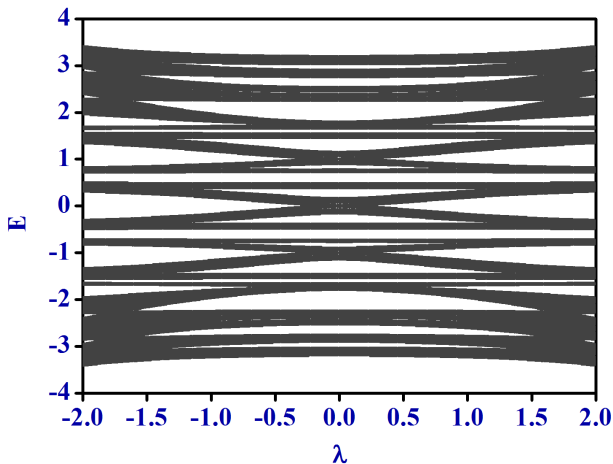


FIG. 5: (Color online) Distribution of energy eigenvalues spectrum of the proposed system as a function of the coupling strength λ . We have chosen $\epsilon_\alpha = \epsilon_\beta = \epsilon_\gamma = \epsilon_0 = 0$, $t_L = 1$, $t_S = 2$, and $\xi = 1$. Number of sites in each side-coupled lower chain is set to 5 and in each upper chain is set to 4.

of an infinite system. In Fig. 5 we observe formation of multiple bands and gaps in the energy eigenvalue spectrum as we vary the value of λ . For values of λ away from $\sqrt{3}$, the spectrum shows the fragmentation with relatively dense packing of energy eigenvalue around certain energy intervals which basically are due to isolated extended states (or, at least states with a large localization length) clustered together. Band-crossing is, in general avoided in such cases. With λ close to the resonance value

of $\sqrt{3}$, absolutely continuous sub-bands start dominating the spectrum, and multifractality disappears.

IV. TWO TERMINAL TRANSMISSION CHARACTERISTICS

To obtain the the two-terminal transmission characteristics of the system, we clamp the system between two semi-infinite ordered leads, viz., source and drain (Fig. 6). The leads are characterized by uniform on-site potential $\epsilon_{\mathcal{L}}$ and nearest neighbor hopping integral $\tau_{\mathcal{L}}$. We renor-

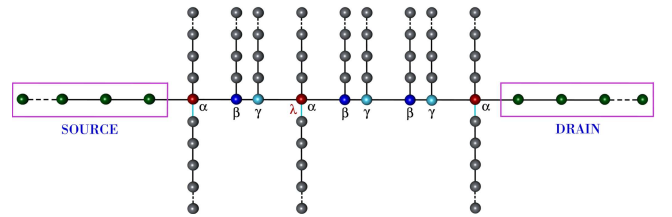


FIG. 6: (Color online) Schematic view of the system clamped between two semi-infinite ordered leads, viz., source and drain.

malize the system clamped between the two leads into an effective dimer by decimating out the internal sites selectively. To get unique recursion relations at the two boundary sites of the system, we consider system with odd generation index only. This should be appreciated that, as we interested to look at the behavior of transmission characteristics of a large finite size system, by choosing system with odd generation index only we do not lose any physics whatsoever. Instead of deflation rule used in Sec. II B, we now use an alternative deflation rule $LSL \rightarrow L'$ and $LS \rightarrow S'$ [10]. By using this deflation rule, starting with an $(2n + 1)$ -th generation Fibonacci system, decimation of n steps converts it into an effective dimer with two renormalized atomic sites having effective on-site potentials $\tilde{\epsilon}_l^*$ and $\tilde{\epsilon}_r^*$ (for the “left” and “right” edge sites) and are connected to each other by an effective hopping integral t_L^* . The recursion relations arises out of this decimation procedure are given by,

$$\begin{aligned}
 \tilde{\epsilon}_{\alpha,n} &= \tilde{\epsilon}_{\alpha,n-1} + \frac{\mathcal{X}_{n-1}}{\mathcal{Z}_{n-1}} + \frac{\mathcal{Y}_{n-1}}{\mathcal{Z}_{n-1}} \\
 \tilde{\epsilon}_{\beta,n} &= \tilde{\epsilon}_{\alpha,n-1} + \frac{t_{L,n-1}^2}{E_{\beta,n-1}} + \frac{\mathcal{Y}_{n-1}}{\mathcal{Z}_{n-1}} \\
 \tilde{\epsilon}_{\gamma,n} &= \tilde{\epsilon}_{\gamma,n-1} + \frac{t_{S,n-1}^2}{E_{\beta,n-1}} + \frac{\mathcal{X}_{n-1}}{\mathcal{Z}_{n-1}} \\
 \tilde{\epsilon}_{l,n} &= \tilde{\epsilon}_{l,n-1} + \frac{\mathcal{X}_{n-1}}{\mathcal{Z}_{n-1}} \\
 \tilde{\epsilon}_{r,n} &= \tilde{\epsilon}_{r,n-1} + \frac{\mathcal{Y}_{n-1}}{\mathcal{Z}_{n-1}} \\
 t_{L,n} &= \frac{t_{L,n-1}^2 t_{S,n-1}}{\mathcal{Z}_{n-1}}, \quad t_{S,n} = \frac{t_{L,n-1} t_{S,n-1}}{E_{\beta,n-1}}
 \end{aligned} \tag{7}$$

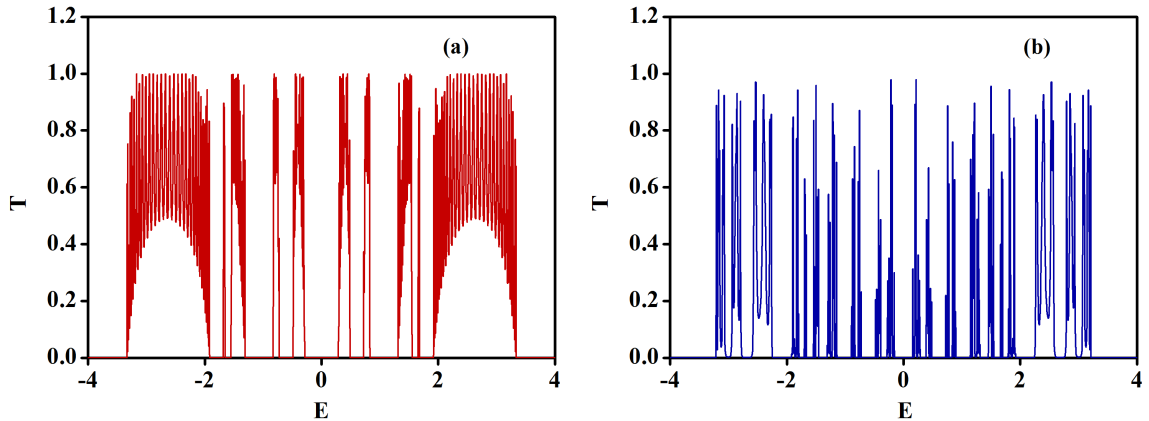


FIG. 7: (Color online) Transmission characteristics of a 9-th generation system as a function of the energy E . (a) represents the transmission characteristics under the resonance condition ($\lambda = \sqrt{3}$) and (b) is for the 50% deviation from the resonance condition. Number of sites in each side-coupled lowerchain is 5 and in each upper chain is 4. The values of other parameters are $\epsilon_\alpha = \epsilon_\beta = \epsilon_\gamma = \epsilon_0 = 0$, $\epsilon_l = \epsilon_r = 0$, $t_L = 1$, $t_S = 2$, and $\xi = 1$. The lead parameters chosen $\epsilon_L = 0$ and $t_L = 2$.

where, $\mathcal{X}_{n-1} = t_{L,n-1}^2 E_{\gamma,n-1}$, $\mathcal{Y}_{n-1} = t_{L,n-1}^2 E_{\beta,n-1}$, $\mathcal{Z}_{n-1} = E_{\beta,n-1} E_{\gamma,n-1} - t_{S,n-1}^2$, and $E_{j,n-1} = (E - \epsilon_{j,n-1})$ for $j = \alpha, \beta, \gamma$. The transmission coefficient across the effective di-atomic system is given by [29],

$$T = \frac{4 \sin^2 ka}{\mathcal{A}^2 + \mathcal{B}^2}$$

with, $\mathcal{A} = [(P_{12} - P_{21}) + (P_{11} - P_{22}) \cos ka]$
and $\mathcal{B} = [(P_{11} + P_{22}) \sin ka]$ (8)

where, $P_{11} = [(E - \tilde{\epsilon}_l^*)(E - \tilde{\epsilon}_r^*)]/t_L^* \tau_L - t_L^*/\tau_L$, $P_{12} = -(E - \tilde{\epsilon}_r^*)/t_L^*$, $P_{21} = (E - \tilde{\epsilon}_l^*)/t_L^*$, $P_{22} = -\tau_L/t_L^*$ are the matrix elements of the transfer matrix for the effective di-atomic system, and $\cos ka = (E - \epsilon_L)/2\tau_L$, ‘ a ’ being the lattice constant of the leads and is set to unity throughout the calculation.

In Fig. 7 we have presented the transmission characteristics of a 9-th generation system. As we tune the value of λ to $\sqrt{3}$, which is the resonance value of λ , the transmittance of the system gets enhanced significantly as apparent from Fig. 7(a). This result is at par with the results discussed in Sec. III and confirms the extended character of the corresponding electronic eigenstates. The oscillation in the T - E profile is due to the finite dangling chains, where a standing wave pattern is formed. In Fig. 7(a) we observe several high-transmission zones separated by zero-transmission zones. This feature can be useful in designing small scale novel filtering devices with such systems. The effect of deviation from the resonance condition on the transmission coefficient T is shown in Fig. 7(b), where we have chosen $\lambda = \sqrt{3}/2$, which is the 50% deviated value of λ from its resonance value. The transmission characteristics under this condition exhibit a highly fluctuating behavior indicating poor conducting nature of a quasiperiodic system in general. Sudden bursts of transmission peaks are due to the formation of isolated extended states as mentioned earlier.

V. CONCLUSION

In conclusion, we have studied the electronic energy spectrum and transmission characteristics of a model Fibonacci quasiperiodic system with side-coupled periodic QD arrays within a tight-binding framework. The local density of states and the transmission coefficient are computed using an RSRG analysis. The major result is that, we are able to find a certain relationship between the parameters of the Hamiltonian of the system, which triggers absolutely continuous subbands in the energy spectrum of the system. The extended nature of the electronic states under the suitable resonance condition is affirmed by a prominent enhancement in the transmission coefficient. The number and the position of the continuous subbands can be controlled by tuning the number of atomic sites in the side-attached chains. This opens up a possibility of devising nanoscale electronic filtering devices with such systems. We have investigated the effect of side-attachments on a Fibonacci type backbone – this study can be carried over to some other quasiperiodic structures like copper mean, Thue-Morse etc. with side-attached periodic chains.

Before we end, it is to be appreciated that the central method presented in this communication is applicable to a variety of building blocks arranged in a completely disordered fashion. The results indicate a unique delocalization of electronic state contrary to the canonical case of Anderson localization.

Acknowledgments

The author is thankful to Prof. Arunava Chakrabarti for his illuminating comments and suggestions during the preparation of the manuscript and acknowledges DST, India for providing funding through an INSPIRE fellow-

ship.

-
- [1] A. E. Miroshnichenko and Y. S. Kivshar, Phys. Rev. E **72**, 056611 (2005).
- [2] A. E. Miroshnichenko, S. Flach, and Y. S. Kivshar, Rev. Mod. Phys. **82**, 2257 (2010).
- [3] P. A. Orellana, G. A. Lara, and E. V. Anda, Phys. Rev. B **74**, 193315 (2006).
- [4] R. Franco, M. S. Figueira, and E. V. Anda, Phys. Rev. B **73**, 195305 (2006).
- [5] A. A. Aligia and L. A. Salguero, Phys. Rev. B **70**, 075307 (2004).
- [6] K. Kobayashi, H. Aikawa, A. Sano, S. Katsumoto, and Y. Iye, Phys. Rev. B **70**, 035319 (2004).
- [7] P. A. Orellana, F. Domínguez-Adame, I. Gómez, and M. L. Ladrón de Guevara, Phys. Rev. B **67**, 085321 (2003).
- [8] V. Pouthier and C. Girardet, Phys. Rev. B **66**, 115322 (2002).
- [9] Z. -Y. Zhang, S.-J. Xiong, and S. N. Evangelou, J. Phys.: Condens. Matter **10**, 8049 (1998).
- [10] A. Chakrabarti, Phys. Rev. B **74**, 205315 (2006).
- [11] A. Chakrabarti, Phys. Lett. A **366**, 507 (2007).
- [12] U. Fano, Phys. Rev. **124**, 1866 (1961).
- [13] F. Haupt, S. Smolka, M. Hanl, W. Wüster, J. Miguel-Sanchez, A. Weichselbaum, J. von Delft, and A. Imamoglu, Phys. Rev. B **88**, 161304(R) (2013).
- [14] N. Zuniga-Hansen, Y.-C. Chi, and M. S. Byrd, Phys. Rev. A **86**, 042335 (2012).
- [15] J.-X. Zhu, J.-P. Julien, Y. Dubi, and A. V. Balatsky, Phys. Rev. Lett. **108**, 186401 (2012).
- [16] M. Kohmoto, L. P. Kadanoff, and C. Tang, Phys. Rev. Lett. **50**, 1870 (1983).
- [17] J. B. Sokoloff, Phys. Rep. **126**, 189 (1985).
- [18] M. Kohmoto, B. Sutherland, and C. Tang, Phys. Rev. B **35**, 1020 (1987).
- [19] E. Maciá and F. Domínguez-Adame, *Electrons, Phonons and Excitons in Low Dimensional Aperiodic Systems* (Editorial Complutense, Madrid, 2000).
- [20] G. G. Naumis, Phys. Rev. B **59**, 11315 (1999).
- [21] C. Forestiere, G. Miano, G. Rubinacci, and L. Dal Negro, Phys. Rev. B **79**, 085404 (2009).
- [22] C. Forestiere, G. Miano, C. Serpico, M. d'Aquino, and L. Dal Negro, Phys. Rev. B **79**, 214419 (2009).
- [23] L. Dal Negro and Ning-Ning Feng, Optics Express **15**, 14396 (2007).
- [24] A. Gopinath, S. V. Boriskina, B. M. Reinhard, L. Dal Negro, Optics Express **17**, 3741 (2009).
- [25] N. E. Kaputkina, Yu E. Lozovik, R. F. Muntyanu, and Yu Kh Vekilov, J. Phys.: Conf. Ser. **226**, 012028 (2010).
- [26] P. W. Anderson, Phys. Rev. **109**, 1492 (1958); P. A. Lee and T. V. Ramakrishnan, Rev. Mod. Phys. **57**, 287 (1985).
- [27] A. Chakrabarti, S. N. Karmakar, and R. K. Moitra, Phys. Rev. B **39**, 9730 (1989).
- [28] S. Jana and A. Chakrabarti, Phys. Rev. B **77**, 155310 (2008).
- [29] A. D. Stone, J. D. Joannopoulos, and D. J. Chadi, Phys. Rev. B **24**, 5583 (1981).